An accurate new method to measure the dimensionless figure of merit of thermoelectric devices based on the complex impedance porcupine diagram

An accurate new method to measure the dimensionless figure of merit of thermoelectric devices based on the complex impedance porcupine diagram

Andrea De Marchi[1,2] and Valter Giaretto[2,3]
[1]*Dipartimento di Elettronica, Politecnico di Torino, C.so Duca degli Abruzzi, 24, 10129 Torino, Italy*
[2]*Consorzio Nazionale Interuniversitario di Scienze fisiche della Materia (CNISM), Unità di Ricerca Politecnico di Torino C.so Duca degli Abruzzi, 24, 10129 Torino, Italy*
[3]*Dipartimento di Energetica, Politecnico di Torino, C.so Duca degli Abruzzi, 24, 10129 Torino, Italy*

(Received 28 June 2011; accepted 6 October 2011; published online 28 October 2011)

The heat diffusion related $f^{-1/2}$ slow decay in the frequency domain transfer function of thermoelectric devices introduces a bias in figure of merit measurement methods that do not take it into account. The bias can range from less than 1% to more than 20% depending on the device. Harman type methods are not immune. Neither is the simple single measurement procedure proposed here on the basis of a complex thermal impedance analysis of the device, but in this case the supporting theory allows evaluating and correcting for the bias with documented accuracy. To this aim, both a theoretical approach based on *a priori* knowledge of the device and an experimental one based on theory guided measurements are possible and are described in the paper. Typical residual Type B uncertainties after correction can be below 10% of the bias. © *2011 American Institute of Physics*. [doi:10.1063/1.3656074]

I. INTRODUCTION

Thoroughly characterizing thermoelectric materials and devices is no easy task as it involves measuring both thermal and electrical quantities as well as thermoelectric parameters connecting the two worlds. A shortcut which has been found practical is to measure the dimensionless figure of merit zT instead of the whole set of such quantities. In fact, it is mostly on the basis of this parameter that a judgment can be made on the overall quality of thermoelectric materials and devices as employed in practical applications.

While the intrinsic thermoelectric material's figure of merit is defined as $zT = \varepsilon^2 T/(\lambda\rho_e)$, where ε is the single-junction Seebeck coefficient, λ and ρ_e are the material's thermal conductivity and electrical resistivity, respectively, and T is the average sample's temperature, the relevant quality indicator for a real practical realization is

$$zT = \frac{\varepsilon^2 T}{\mathscr{R}\mathscr{K}} \tag{1}$$

where $\mathscr{K}$ and $\mathscr{R}$ are the total thermal conductance and the total series electrical resistance of the device. Only for a single leg in ideal conditions does this coincide with the material's intrinsic figure of merit, as in this case is $\mathscr{R} = \rho_e 2L_0/A$ and $\mathscr{K} = \lambda A/2L_0$, if $2L_0$ and A are length and cross section of the thermoelectric element.

The practically relevant value of Eq. (1) is also what can be evaluated in a real device by measuring electrical quantities at the accessible external connections, because it can be obtained as the ratio between the total developed Seebeck voltage V_ε and the total ohmic voltage drop V_Ω,

$$zT = \frac{V_\varepsilon}{V_\Omega} = \frac{\varepsilon\,\Delta T}{\mathscr{R}\,Ai} = \frac{\varepsilon\,\Pi}{\mathscr{R}\mathscr{K}} = \frac{\varepsilon^2 T}{\mathscr{R}\mathscr{K}}, \tag{2}$$

where i is the electric current density and Π the Peltier coefficient.

Separating the two contributions is not trivial and is traditionally performed with some version of a time-domain transient approach[1,2] denominated the "Harman method," which envisions measuring the sudden voltage drop experienced at the terminals of the device when a dc current previously established through it is switched off. The idea behind the method is that, upon switching, the ohmic voltage disappears with the current while the thermoelectric voltage persists as thermal inertia prevents fast temperature variations. Although the correct approach to determine the step response of a system requires anti-transforming a transfer function in the Laplace domain, correct answers are still obtained with that simple method provided the system is dominated by a single pole, which only recently[3] was shown not to be the case in thermoelectric devices.

Several improvements were added over time to this original idea, aimed at keeping in check the effects of Joule heating. Most popular seems to have recently become what has been referred to as "the modified[4–7] Harman method," which has the merit of keeping Joule heating constant throughout the measurement procedure. In order to achieve this goal, the dc current is reversed periodically for some time at some not better specified "high frequency" (which is however low enough to avoid an extra voltage from the series inductance of the device) and then is finally fixed in direction until the transient is extinguished. The ratio between the final asymptotic voltage and half the peak-to-peak voltage measured during the periodic switching phase is taken to be a good evaluation of $1 + zT$. This modified method suffers from the existence of the half pole in the transfer function, demonstrated in Ref. 3, because the device's response does not decay with frequency as fast as previously assumed.

Much work has been devoted to the task of studying in detail the corrections that must be introduced onto measured values in order to recover the intrinsic figure of merit of employed thermoelectric materials. Errors caused by heat losses were considered,[8–15] as well as biases from parasitic electrical and thermal contact resistances.[10,12,13] With one notable exception[16,17] no serious efforts seem instead to have been spent in trying to define alternative methods to measure the figure of merit of a thermoelectric device. Apparently, confidence in the method has been so high as to even prompt the realization of Z-meters based on it.[18,19] In order to provide an alternative approach, which is generally suggested by the international metrological community to foster comparisons between results obtained with different accuracy budget structures, in this paper a different method is proposed for the measurement of the figure of merit.

The ratio between junction temperature response and injected Peltier heat flux can be interpreted as the transfer function of a transducer, and in this light was recently presented,[3] but can also be seen as a thermal impedance,[20] and in this meaning will be considered here. A one-dimensional model is adopted, in which three-dimensional constriction and spreading resistances are treated as in Ref. 3 and contact resistances between different layers are not considered. These assumptions were shown in Ref. 3 to lead to analytical results consistent with experimental data, which confirms their adequacy. The heat diffusion equations are solved with the complex phasor method[21] assuming suitable boundary conditions.

Diagrams obtained for the impedance in the complex plane turn out to be suggestive of a porcupine profile, which prompted for them the sticky nickname of "porcupine diagrams." They are helpful for the evaluation of the figure of merit with new strategies, and indicate with graphic evidence that in some cases the Harman method may be affected by even quite relevant undetected biases, which can be avoided with the new approach discussed in this paper.

The new proposed method is applied here in basically isothermal conditions to obtain what could be called a "small signal" figure of merit, but could also be applied to a device exposed to environments at different temperature on the two sides to obtain a figure of merit valid for that temperature difference, which would include the Thomson effect. This is an important piece of information, as pointed out in Ref. 17.

In the following, analytical solutions will first be developed in Sec. II for the lumped parameters model, in order to establish a historical reference for the new method, while in Sec. III the complex phasor method is applied to a distributed model in order to characterize the errors ingrained in the lumped approach. A discussion on the use of porcupine diagrams for zT evaluation will be given in Sec. IV.

II. THE LUMPED PARAMETERS MODEL

For the mentioned continuity reasons, the complex phasor symbolism is here first applied to the lumped parameters model, which is the practical description of the single thermal pole assumption that was historically considered valid for thermoelectric devices.

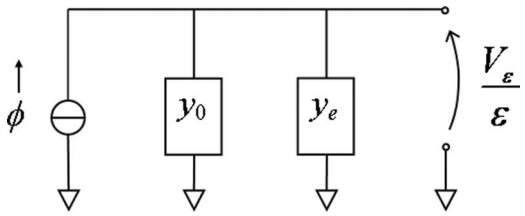

FIG. 1. Electrical equivalent of the thermal circuit of the thermoelectric device. The Seebeck voltage is indicated to underline the fact that the device is observed at the junctions.

The equivalent electrical circuit representation shown in Fig. 1 will be used for the one-dimensional model of the thermoelectric device. Quantities here are all per-unit-area, and the effects of spreading and constriction resistances at physical interfaces, discussed in Ref. 3, are assumed to be taken into account. As such, the generated Peltier heat flux density $\phi = \Pi i$ is referred to the current density i, while K_0 and C_T are, respectively, the frontal thermal conductance of the thermoelectric element and the frontal thermal capacity of the external layers (electrical connections and thermal insulator). It should be helpful to underline here that K_0 is the conductance of only half of the element, because the device is considered symmetrically conditioned for simplicity, which means that $K_0 = \lambda_0 / L_0$. The current density will be identified here by i because the more commonly used symbol j is dedicated to the imaginary unit $\sqrt{-1}$.

By introducing the total complex thermal admittance y_T, the equivalent circuit yields

$$\frac{V_\varepsilon(\omega)}{\varepsilon\,\phi} = \frac{1}{y_T} = \frac{1}{y_0 + y_e} = \frac{1}{K_0 + j\omega C_T} = \frac{1}{K_0}\frac{1}{1 + j\omega/\omega_{p\ell}} = \frac{1}{K_0}\left(\frac{1}{2} + \frac{1}{2}e^{-j2\psi_\ell}\right), \tag{3}$$

where $\omega_{p\ell} = K_0/C_T$ is the angular frequency of the thermal pole and $\psi_\ell = \text{arctg}\,(\omega/\omega_{p\ell})$. It can be easily seen that this is a half circle in the complex plane, as shown in Fig. 2.

The measured voltage drop V_P and the Seebeck voltage V_ε can then be represented in the complex voltage plane as reported in Fig. 3, where V_Ω is assumed independent of frequency and no contribution of the series inductance is considered, as it becomes relevant at frequencies higher than those considered in this paper.

The figure of merit $V_\varepsilon\,(0)/V_\Omega$ can be obtained by measuring some well identifiable quantity which defines the proportion of the circle to V_Ω. For example one can measure

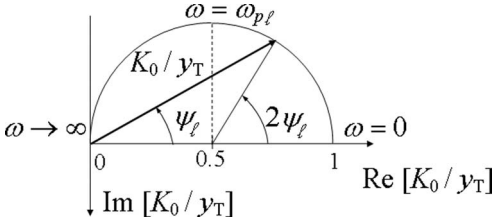

FIG. 2. Diagram as a function of frequency of the complex thermal impedance normalized to the dc thermal resistance, in the lumped parameter approximation.

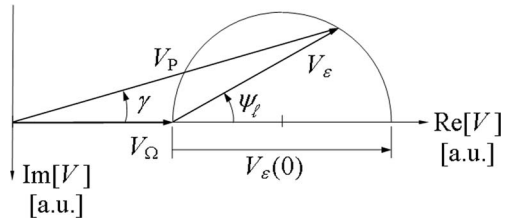

FIG. 3. Diagram of the complex voltage at the electrical terminals of the device.

γ_M, the maximum phase between V_P and V_Ω, as shown in Fig. 4.

In fact, V_ε (0) and V_Ω can be easily related to γ_M, obtaining

$$V_\varepsilon(0) = 2V_P \tan \gamma_M, \tag{4}$$

$$V_\Omega = \frac{V_P}{\cos \gamma_M} - \frac{V_\varepsilon(0)}{2}, \tag{5}$$

and the figure of merit zT^* in the lumped parameter assumption is then obtained as

$$zT^* = \frac{2 \sin \gamma_M}{1 - \sin \gamma_M}. \tag{6}$$

This shows that, given the improved insight offered by the powerful phasor symbolism, a single measurement can be recognized to be sufficient to evaluate the figure of merit in the lumped parameters approximation. Since all what counts is the aspect ratio in Figs. 3 and 4, it is not necessary to combine information obtained from measurements in two different conditions.

The uncertainty of zT^* determination by Eq. (6) relies solely on the accuracy of the maximum phase measurement, for the Type B contribution, and on phase resolution $\delta\gamma$ for the Type A.

The former can be guaranteed to an unnecessary degree by referring to a quartz oscillator, the employed low frequency sine wave synthesizer, and measuring time delays both at rising and falling edges. In fact, the phase difference calculated from the average of these two time intervals discriminates against distortions (typically of the second harmonic type) which may be produced in the device, for example, by Joule heating.

The latter can be easily reduced below 1 mrad, at the very low frequencies at which γ_M occurs (typically below 0.1 Hz), as far as the contribution of the time interval counter resolution is concerned. In fact, counting at 1 kHz is sufficient to guarantee $\delta\gamma < 1$ mrad at the foreseeable maximum frequency of 0.1 Hz. Little more care must be put in making sure that also the single-shot noise contribution to $\delta\gamma$ be adequately small, because averaging many measurements for noise reduction is out of the question for time reasons at these low frequencies.

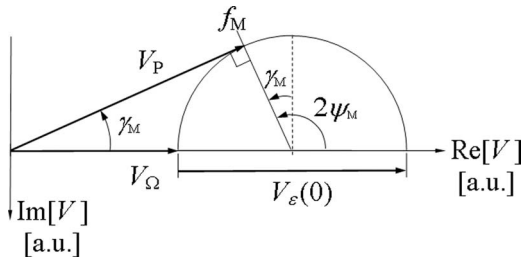

FIG. 4. Complex voltage diagram with indication of quantities γ_M, ψ_M, and f_M used in the determination of the figure of merit zT^*.

Since such noise generated contribution $\delta\gamma$ is the reciprocal of the amplitude signal-to-noise ratio, the latter must be greater than 60 dB for a Type A phase uncertainty smaller than 1 mrad. This imposes a minimum of 10 bit for the digital sine wave synthesizer, and suitably low-noise electronics in the driving circuits.

Given all the above, the limiting Type A uncertainty in the zT^* determination can be derived from Eq. (6) with the usual propagation rules, and is

$$\frac{\delta zT^*}{zT^*} = \frac{\delta\gamma}{(1 - \sin \gamma_M) \tan \gamma_M}. \tag{7}$$

This is a monotonically decreasing function of zT^* which is definitely smaller than $4\delta\gamma$ for $zT^* > 1$.

As a result, the conclusion can be made that 0.5% uncertainty can be achieved with this approach in the measurement of zT^*.

Alternatively, one can choose to measure other quantities in easily identifiable points of the circle, for example, V_P and its quadrature component at $\omega = \omega_p$, where the latter is maximized, or V_P at $\omega = 0$ and at $\omega \to \infty$, which in some sense was Harman's choice, as made explicit in Ref. 6.

The advantage of choosing γ_M, besides the single measurement issue, lays both in the precision available for phase measurements and in the fact that the corresponding frequency is relatively high (for a thermal system), which allows to carry out the zT^* evaluation in a relatively short time.

III. THE DISTRIBUTED PARAMETERS MODEL

In the more realistic case of the distributed parameters model, the equivalent circuit of Fig. 1 can be still used, but thermal impedances of thermoelectric elements ($1/y_0$) and external layers ($1/y_e$) must be calculated by solving the heat diffusion equation, which will be done here with the complex phasor method with reference to the geometric scheme of Fig. 5.

With this approach, the heat diffusion equation for the thermoelectric layer can be written as

$$\frac{d^2\vartheta(x)}{dx^2} - \frac{1}{L_0^2}\frac{j\omega}{\omega_0}\vartheta(x) = 0, \tag{8}$$

where ϑ is the temperature excess from the symmetry plane and

$$\omega_0 = \frac{\alpha_0}{L_0^2} = \frac{K_0}{C_0} \tag{9}$$

is the characteristic frequency of the half elements. Equation (8) admits solutions of the form

$$\vartheta(x) = a \exp\left(\frac{x}{L_0}\sqrt{j\omega/\omega_0}\right) + b \exp\left(-\frac{x}{L_0}\sqrt{j\omega/\omega_0}\right), \tag{10}$$

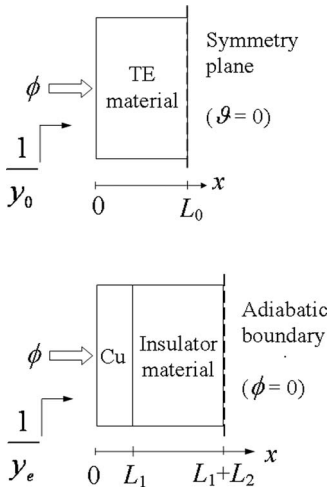

FIG. 5. One-dimensional physical model of the device used for the calculation of thermal impedances in the distributed parameters case.

where the a and b coefficients must be determined with the boundary conditions

$$-\left.\frac{d\vartheta}{dx}\right|_{x=0} = \frac{\phi}{\lambda_0}, \qquad \vartheta(L_0) = 0. \tag{11}$$

The solution for $\vartheta(0)/\phi = 1/y_0$ is

$$\frac{K_0}{y_0} = \frac{\tanh\sqrt{j\omega/\omega_0}}{\sqrt{j\omega/\omega_0}}. \tag{12}$$

For the external impedance, the same procedure must be applied with boundary conditions

$$-\left.\frac{d\vartheta}{dx}\right|_{x=0} = \frac{\phi}{\lambda_1}, \qquad \left.\frac{d\vartheta}{dx}\right|_{x=L_1+L_2} = 0, \tag{13}$$

where L_1 and L_2 are the thicknesses of conducting and insulating layers, and the imposition of temperature and flux continuity at the interface ($x = L_1$).

The solution for $\vartheta(0)/\phi = 1/y_e$ is

$$\frac{K_0}{y_e} = \frac{1 + \frac{K_2}{K_1}\sqrt{\omega_1/\omega_2}\tanh\sqrt{j\omega/\omega_1}\,\tanh\sqrt{j\omega/\omega_2}}{\frac{K_1}{K_0}\sqrt{j\omega/\omega_1}\tanh\sqrt{j\omega/\omega_1} + \frac{K_2}{K_0}\sqrt{j\omega/\omega_2}\tanh\sqrt{j\omega/\omega_2}}, \tag{14}$$

where the characteristic frequencies ω_1 and ω_2 are defined similarly to ω_0 in Eq. (9).

The equivalent circuit is solved like in the lumped parameters case, with the total complex thermal admittance $y_T = y_0 + y_e$ given in this case by a suitable combination of Eqs. (12) and (14).

The difference between the two approaches, in the low frequency range, can be quantified if the hyperbolic tangents appearing in y_T are approximated with their third-order expansion. An expression is obtained which can again be shown to be a circle in the complex impedance plane, like it was in the lumped parameters case, with the noticeable difference that the radius is smaller and the centre is shifted.

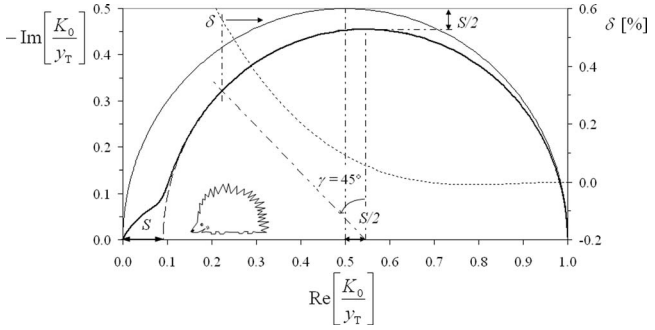

FIG. 6. Example of porcupine diagram of the normalized complex thermal impedance of a thermoelectric device (thick solid line), with indication of the lumped approximation (thin solid line) and the body approximating half circle (dashed line). The curve δ (dotted line) represents the relative radial distance of the porcupine body from the latter circle.

In fact, the following form can be given to the expression of the impedance:

$$\begin{aligned}\frac{K_0}{y_T} &= \frac{K_0}{y_0 + y_e} = \frac{1 + S(j\omega/\omega_p)}{1 + j\omega/\omega_p} \\ &= \frac{1+S}{2} + \frac{1-S}{2}\frac{1 - j\omega/\omega_p}{1 + j\omega/\omega_p} \\ &= \frac{1+S}{2} + \frac{1-S}{2}e^{-j2\psi},\end{aligned} \tag{15}$$

where S is given by

$$\begin{aligned}\frac{S}{\omega_p} &= \frac{1}{\omega_1}\frac{C_2}{C_1} + \frac{1}{3}\frac{1}{C_1 + C_2}\left(\frac{C_1}{\omega_1} + \frac{C_2}{\omega_2}\right) \\ &= \frac{C_2}{K_1} + \frac{1}{3}\frac{C_1}{K_1}\frac{C_1}{C_1 + C_2} \\ &\quad + \frac{1}{3}\frac{C_2}{K_2}\frac{C_2}{C_1 + C_2},\end{aligned} \tag{16}$$

and the angle

$$\psi = \mathrm{arctg}\left(\frac{\omega}{\omega_p}\right) \tag{17}$$

is still formally related to frequency in the same way as in the lumped model. However, the value of the thermal pole angular frequency ω_p is lower than the $\omega_{p\ell} = K_0/(C_1+C_2)$ value that it had in that case. In fact, the pole frequency is reduced according to

$$\frac{1}{\omega_p} = \frac{1}{\omega_{p\ell}} + \frac{1}{3\omega_0} + \frac{S}{\omega_p} \approx \frac{1}{\omega_{p\ell}} + \frac{S}{\omega_p}, \tag{18}$$

where the approximation is particularly good for shorter thermoelectric elements, for which $\omega_0 \gg \omega_p$.

How close the half circle of Eq. (15) is to the impedance diagram obtained from Eqs. (12) and (14) is shown in Fig. 6 for an actual device (as described in its commercial datasheet), in which the departure from the lumped parameters model is quite evident. Alumina, Copper, and Bi_2Te_3 are assumed to be the materials of the device, whose geometry is defined by $L_0 = 0.1$ mm, $L_1 = 0.01$ mm, and $L_2 = 0.5$ mm, and an area filling factor of 0.5.

The curve of the total impedance in the complex plane changes from the half circle of the lumped parameters model (shown for comparison) into a shape that looks like the profile of a porcupine (also shown for comparison). In the following we will refer to this representation as the porcupine diagram. The body of the porcupine corresponds to the frequency range dominated by the thermal pole, while the snout corresponds to the high frequency half pole section.[3] The parameter S is the ratio between the length of the snout and the length of the whole porcupine.

The relative departure of the actual calculated body profile from the approximating half circle is also characterized in Fig. 6 by the parameter δ, which is the local radial distance of the body from the circle, referred to its radius. The reported dotted curve represents δ as a function of the value of $\mathrm{Re}[K_0/y_T]$ in the considered point on the circle. It can be seen that δ is always smaller than 0.6% in the considered case for γ values smaller than 45°. With the help of Eq. (6) it can be figured out that this phase angle range corresponds to the figure of merit range $zT^* < 5$ if γ is interpreted as γ_M, the maximum phase used to evaluate zT^*. This information will be used in Sec. IV to discuss the uncertainty that it introduces, which will be shown to be acceptable.

In Fig. 7(a) the Bode diagram of the calculated absolute value of the thermal impedance $1/y_T$ is reported in arbitrary units for different values of L_0 and constant typical values for all the others quantities defining the thermoelectric device; similarly, the effect of varying L_2 with everything else constant is shown in Fig. 7(b). Incremental steps are here a factor of $\sqrt{10}$ in both cases.

It can be seen that the half pole section of the diagram, which generates the porcupine's snout, is common to all curves, irrespective of L_0 and L_2. This derives from the fact that both insulating and thermoelectric layers are thermally thick in that region, which makes their thermal impedance close to their respective characteristic impedance[20] $(\sqrt{j\omega}\,e)^{-1}$, where e is the thermal effusivity of the material. As a result, as long as the copper layer is thermally thin, in that frequency range it is

$$\frac{1}{y_T} \approx \frac{1}{\sqrt{j\omega}\,(e_0 + e_2)}. \tag{19}$$

This approximation can also be easily derived analytically from Eqs. (12) and (14), as already pointed out in Ref. 3.

Incidentally, it is interesting to point out that the angular frequency at which the Bode diagram changes slopes is approximately ω_2, as indicated in Fig. 7(a). This can be derived by comparing Eq. (19) with Eq. (3) and assuming $e_2 \gg e_0$ and $\omega \gg \omega_{p\ell}$.

In the thermal pole dominated region, instead, all curves in Fig. 7(a) eventually flatten out to a level proportional to L_0, at angular frequencies lower than ω_p. As it turns out, both ω_p and S are proportional to $1/L_0$, while $S \propto L_2$ and $\omega_p \propto 1/L_2$.

In Fig. 8, two complex thermal impedance diagrams are shown, which qualitatively characterize how the Bode diagram variations of Fig. 7 translate in the porcupine representation. Incremental steps given to L_0 in Fig. 8(a) and L_2 in Fig. 8(b) are only 12.2% for obvious graphical reasons. Such steps are ten times smaller, in a logarithmic scale, than those used in Fig. 7. In both cases, it is evident from the figures that the relative snout length S changes in the same 12.2% proportion at each step. Also shown in the diagrams is the different way in which the frequency parameter slides along the porcupine for changing L_0 and L_2 values.

Since the tip of the snout corresponds to $\omega \to \infty$, it is evident from Figs. 6–8 that measuring what is commonly denominated "the ac resistance" in the modified Harman method[4–7] runs the risk to include in the value taken to be the ohmic

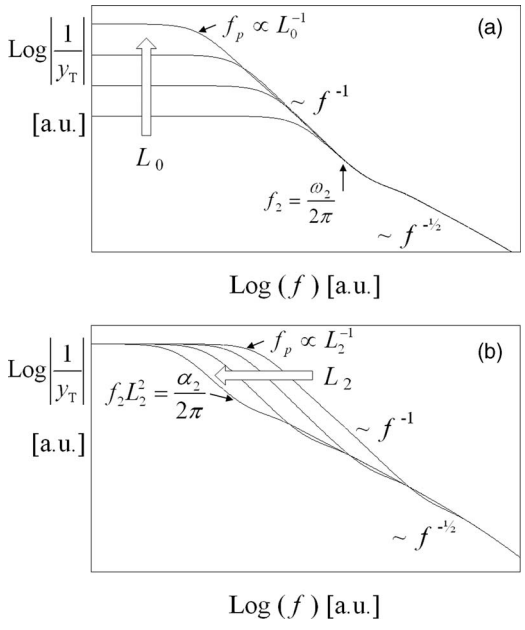

FIG. 7. (a) Effect of L_0, (b) effect of L_2 on the transfer function Bode diagram of a thermoelectric device. Thickness values are varied in steps of 10 dB (~200%).

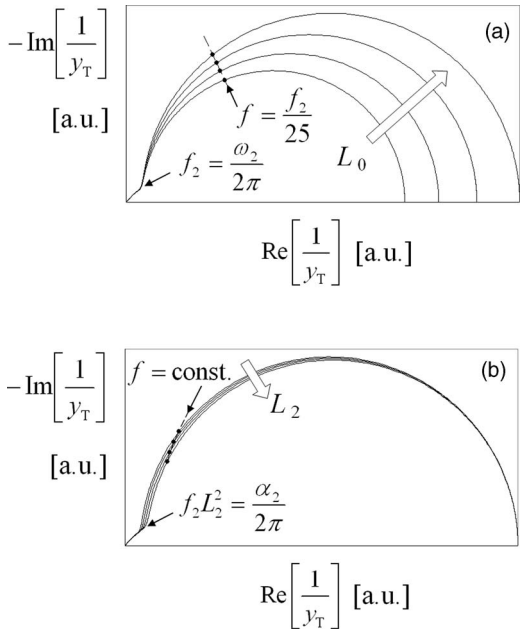

FIG. 8. (a) Effect of L_0, (b) effect of L_2 on the porcupine diagram of a thermoelectric device. Thickness values are varied in steps of 1 dB (~12.2%).

voltage a contribution from the snout of the porcupine. The corresponding error will depend on the frequency at which such measurement is actually performed. However, since the half pole decay in the frequency domain is slow, unreasonably high frequencies may be necessary to reduce it significantly. On the other hand, thinking of the original transient Harman method, one should consider that the half pole in the high frequency region dominates the first part of the step response of the system. Since the latter introduces a transient signal which starts with a theoretically infinite slope,[22] it is impossible to spot its contribution and separate it from the ohmic voltage.

As a matter of fact, any measurement method which does not properly account for the snout would yield biased values for the dimensionless figure of merit, with greater biases for devices with shorter thermoelectric elements and thicker insulators.

In all cases the figure of merit comes out underestimated in the process, which makes the possibility to correct for this bias very appealing.

IV. FIGURE OF MERIT EVALUATION WITH PORCUPINE DIAGRAMS

Once realized with the distributed parameters analysis that the impedance diagram of a thermoelectric device in the complex plane is not a half circle, but rather a porcupine-like profile, it becomes obvious that the simple approach of measuring γ_M and inserting it in Eq. (6) yields a value for the figure of merit which is potentially biased and may have to be corrected in order to meet the desired accuracy. The advantage of the method here proposed lays also in the fact that the "snout error" is well defined and the correction can then be made with documented accuracy.

Two biases must be considered. The lesser one stems out of the relative distance δ of the porcupine body from circularity (shown in Fig. 6) which biases γ_M and as a consequence also zT^*. This error is always positive and can be estimated by applying Eq. (7), which is written for the propagation of the uncertainty $\delta\gamma$, to the propagation of the bias $\Delta\gamma$. The latter can be calculated by considering that $\delta = \Delta\gamma/\tan(\gamma_M)$. Further attention will be given to it later, when discussing the overall uncertainty of the proposed measurement method.

The main bias is generated by the relative length S of the porcupine's snout. In fact, if the latter is taken into account, the figure of merit $zT = V_\varepsilon(0)/V_\Omega$ of the device can be written as

$$zT = zT^* \frac{1+S^*}{1-S^* zT^*} = zT^* \frac{1}{1-S(1+zT^*)}, \tag{20}$$

where $S^* = S/(1-S)$ is the length of the snout referred to the diameter of the circle which approximates the porcupine's body. The parameter S^* is introduced because, contrary to S, it is normalized with respect to a quantity which can be evaluated with Eq. (4). It must however be underlined that the zT^* definition used do derive Eq. (20) is not the one given in Eq. (6), but rather one similar to the definition of zT given in Eq. (2), with $V_\varepsilon(0)$ and V_R, respectively, reduced and increased of the snout. The two definitions of zT^* differ because of the above mentioned body circularity error. If Eq. (20) is used to derive zT from a zT^* value based on measured γ_M and Eq. (6), which is its only available estimate, the obtained result must be corrected for both biases.

The relative "snout correction" can be derived from Eq. (20) itself, and is given by

$$\frac{zT - zT^*}{zT^*} = \frac{S^*(1+zT^*)}{1-S^* zT^*} = \frac{S(1+zT^*)}{1-S(1+zT^*)}, \tag{21}$$

which shows that the true value of zT is always greater than zT^*. While Eq. (21) is the actual correction needed in the proposed method, how much of this error is actually included in a measurement of the Harman type depends on the fraction of the snout signal contribution that is mistakenly attributed to the ohmic drop in the specific case.

If the snout is small, like it can be in many devices with few mm long thermoelectric elements, the error is not too great, although it can easily be of a few percent. In devices built with short thermoelectric elements, instead, Eq. (21) shows the risk of an important underevaluation of zT. In fact, the snout can easily be of the order of 10% of the body in thin devices, and if zT^* is of the order of 1 this can amount to an underevaluation of the true value by more than 20%.

It is therefore very important to find a way to estimate either theoretically or experimentally the length of the porcupine's snout.

An *a priori* evaluation of the snout's length can be obtained from Eqs. (16) and (18) if geometry and materials are well known, as could be the case of a manufacturer. With this approach, a reasonably good estimate of S can also be obtained, if resistance spreading is taken into account,[3] by approximating ω_p with $\omega_{p\ell} \approx K_0/(C_1+C_2)$, and keeping for S only the third term in Eq. (16). The latter in fact prevails on the first two terms when $L_2 > L_1$, which is the case for modules with typical insulating plates. This fact is shown in Fig. 9, where the respective ratios r' and r'' of the first two terms to the third in Eq. (16) are plotted versus L_2/L_1 for a typical device. With this approximation, the relative snout length S can be expressed as

$$S \approx \frac{\omega_p}{3\omega_2}\left(1+\frac{C_1}{C_2}\right)^{-1} = \frac{1}{3}\frac{K_0}{K_2}\left(1+\frac{C_1}{C_2}\right)^{-2}$$

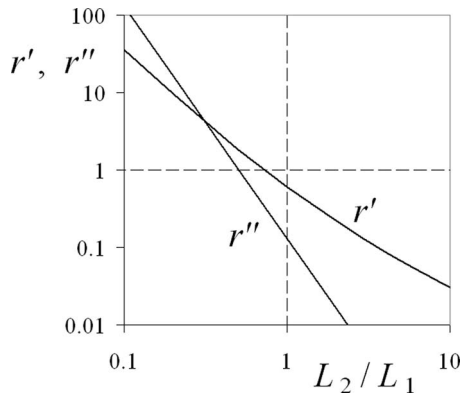

FIG. 9. Weights r' and r'' of the first two terms in Eq. (16) relative to the third, as a function of L_2/L_1, for the device of Fig. 6.

$$= \frac{1}{3}\frac{\lambda_0}{\lambda_2}\frac{L_2}{L_0}\left(1+\frac{\rho c_1}{\rho c_2}\frac{L_1}{L_2}\right)^{-2}, \quad (22)$$

which may not always offer adequate accuracy by itself, but in any case is at least useful for a decision on the need to adopt an experimental approach to determine the snout correction.

On the other hand, if an experimental evaluation of S is judged necessary, a strategy must be devised to optimize the process from the points of view of uncertainty and type and number of needed measurements.

To this aim, the critical point is the fact that the tip of the snout, which is the very point of the diagram whose position is sought, cannot be reached in practice because even getting close to it involves very high frequencies, a region where it is very difficult to properly compensate for the parasitic inductance. The needed strategy must therefore allow one to infer the position of the snout tip from measurements taken at more viable frequencies.

The only possible basis for such a strategy can be the shape of the snout itself. The best bet seems to be to exploit the observation that its profile is generally aligned around thermal impedances with a 45° phase angle, which is where it would be if the module had a single external layer, according to Eq. (19). Actual devices are more complex than that, which leads to geometry dependant snout profiles. A snout length evaluation based on the 45° slope assumption will then introduce a Type B uncertainty contribution. Still, this appears to be the best than can be done, topped only by the possibility to reduce this uncertainty with the help of a model-based calculation of the expected snout profile in the particular device. However, if the device's geometry and materials are so well known as to allow this improvement, it may well be possible to avoid altogether the experimental approach and settle with a snout length evaluation by Eq. (16).

Among other conceivable ways to exploit the expected snout profile, an experimental procedure structured in three steps is here suggested, which has the advantage of looking for extremes of a relevant quantity as a function of frequency.

A block diagram of the assumed measurement system, which is presently in the process of being engineered, is shown in Fig. 10.

For the necessary experimental support to the conceptual developments which are reported here, off the shelf instrumentation was used, and phase shifts were evaluated graphically from Lissajous figures. The phase resolution obtained in this way was limited to about 5 mrad. This is far from the best that can be done, but was still adequate, albeit marginally, to provide experimental support to the present work within its scope.

The suggested experimental procedure will be illustrated here with reference to Figs. 11 and 12, which are based on the calculated porcupine profile for the device of Fig. 6. In Figs. 13 and 14, instead, data points taken in the course of applying this procedure to an available device are compared to the corresponding calculated curves. The geometry of the module is defined by $L_0 = 1.45$ mm, $L_1 = 0.25$ mm, and $L_2 = 0.9$ mm, with an area filling factor[3] of 0.35. As usual, Bi_2Te_3, copper and alumina are assumed to be its materials.

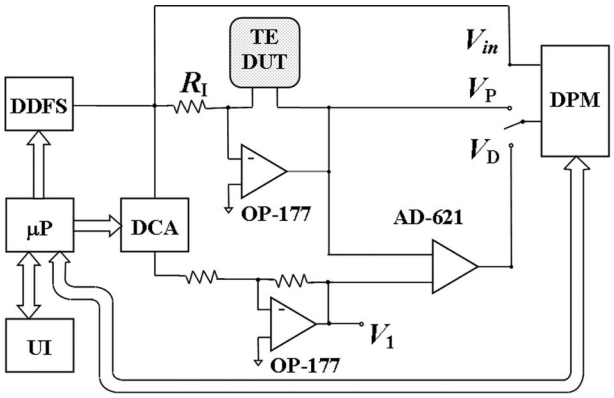

FIG. 10. Block diagram of a possible configuration of an electronic system dedicated to the measurement of the figure of merit of a thermoelectric device. DDFS = direct digital frequency synthesizer, DCA = digitally controlled attenuator, DPM = digital phase meter, μP = micro-processor, UI = user interface, TE DUT = thermoelectric device under test. Operational amplifiers and differential amplifier are selected for low noise and high CMRR. The resistor R_I defines the ratio between the input voltage V_{in} generated by the DDFS and the current fed to the DUT.

The three steps are carried out as follows.

Step 1: The phase angle between the input driving current and the total voltage V_P developed at the terminals of the device is maximized to γ_M by adjusting the frequency of the sine-wave generator, and measured to better than 1 mrad with a digital phase meter (DPM) of the time interval counter type. The frequency f_M at which γ_M is obtained is stored for later use and zT^* is calculated with Eq. (6).

For the experimentally tested device, the mentioned suboptimum instrumentation allowed finding the values $f_M = 9.5$ (0.3) mHz and $\gamma_M = 12.56$ (0.3) deg for these quantities, which yield an estimate of 0.555 (0.016) for zT^*, similar to the values obtained with the transient Harman method and the modified Harman method.

Step 2: The frequency is set to the value f_{45} given by

$$f_{45} = f_M \frac{\tan(3\pi/8)}{\tan(\pi/4+\gamma_M/2)} \quad (23)$$

at which the tangent to the porcupine body has a slope of 45°, as shown in Fig. 11. Equation (23) is derived from Eq. (17) by considering that $2\psi_M = \gamma_M + \pi/2$, as shown in Fig. 4. At

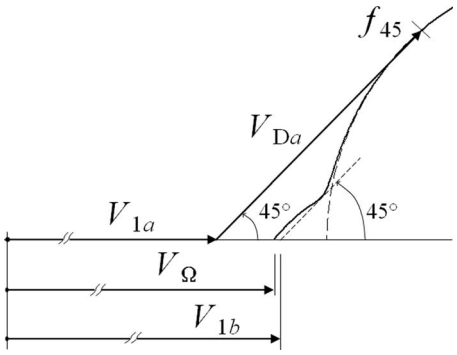

FIG. 11. Diagram of the complex voltage at the electrical terminals of the device around the porcupine snout. The indicated quantities are the ones used in the proposed snout length evaluation procedure.

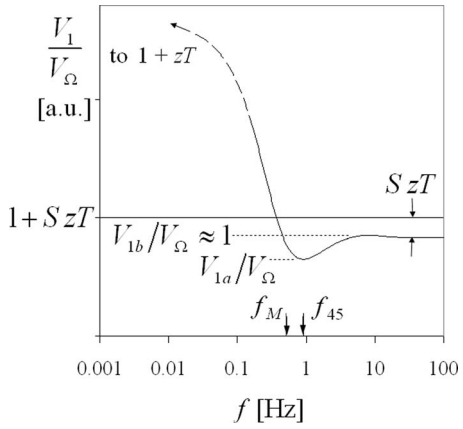

FIG. 12. Plot as a function of frequency, for the device of Fig. 6, of relative V_1 values for which the output V_D of the differential amplifier is 45° out of phase from the injected current.

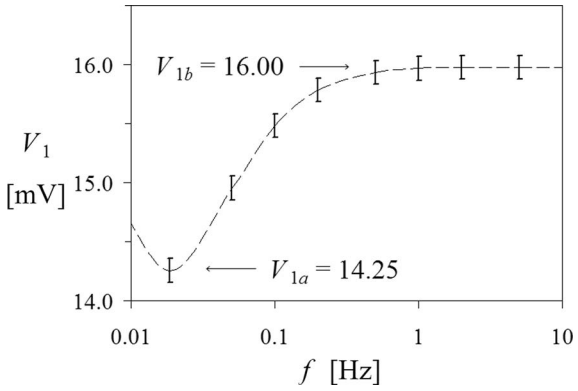

FIG. 14. Values of V_1 for which the output V_D of the differential amplifier was 45° out of phase from the injected current in the course of the evaluation of the available device. The relevant measured values of V_{1a} and V_{1b} are indicated.

this frequency the phase angle between the input current and the output V_D of the differential amplifier is then driven to 45° by adjusting the voltage V_1 of the reference branch, at which point the value V_{1a} of the latter is measured and stored. In Fig. 12 a plot is given, as a function of frequency, of the V_1 values for which V_D is at 45°. It is clear that V_{1a} is the minimum of this function. As a consequence, the uncertainty associated with V_{1a} can be very small even if the frequency f_{45} were not exceedingly precise. Incidentally, it can be noticed that an independent evaluation of zT^* may also be obtained from V_{1a} and the output V_{Da} of the differential amplifier in this situation, divided by its differential gain G. Simple trigonometry is sufficient for this task, yielding

$$zT^* = \frac{2}{\sqrt{2} - 1 + G\frac{V_{1a}}{V_{Da}}}. \tag{24}$$

For the tested module, as shown in Fig. 13, the frequency f_{45} turned out to be 18.5 mHz and the voltage V_{1a} was measured to be 14.25 (0.1) mV_{pp} when the device was driven with a current of 40 mA_{pp}.

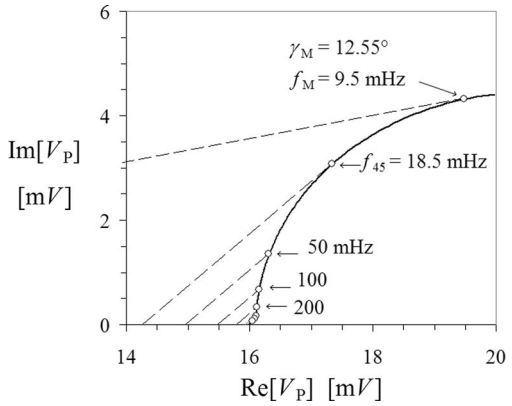

FIG. 13. Measured complex voltages at the electrical terminals of the available device in the course of the suggested three steps procedure for the evaluation of the figure of merit corrected for the porcupine snout. The dashed lines at 45° identify for each frequency the corresponding V_1 value.

Step 3: The frequency is gradually increased and V_1 is adjusted each time to obtain a 45° phase shifted V_D. A possible criterion for the frequency increments can be, for example, to use a geometric progression, namely $f_{k+1} = f_k\ (f_{45}/f_M)$. For the rough test on the available module, the sequence 50, 100, 200, 500 mHz, 1, 2 Hz … was adopted, as shown in Figs. 13 and 14. The process is stopped when the value of V_1 needed to obtain a 45° phase shifted V_D, stabilizes to the maximized value V_{1b} shown in Fig. 12. The latter is taken to be the best possible estimate of the ohmic drop V_Ω. The experimental points tested in applying this process to the evaluated available module are shown in Fig. 14, where the needed peak-to-peak V_1 values at the mentioned frequencies are, respectively, 14.95 mV at 50 mHz, 15.48 mV at 100 mHz, 15.78 mV at 200 mHz, 15.93 mV at 500 mHz, and 16.00 mV from 1 Hz on. The ohmic drop V_Ω , or the measured V_{1b} taken as its proxy, is then seen to be 16.00 (0.10) mV_{pp} with the injected 40 mA_{pp} current, which indicates a series resistance of 0.400 (0.005) Ω.

This information can now be used to substitute for S^* in Eq. (21), obtaining

$$\frac{zT - zT^*}{zT^*} = \frac{\frac{\sqrt{2}-1}{2}(1+zT^*)}{1 - \frac{\sqrt{2}-1}{2}zT^*}\left\{1 - \frac{1 - \frac{V_{1a}}{V_{1b}}}{\frac{\sqrt{2}-1}{2}zT^*}\right\}. \tag{25}$$

The ratio V_{1a}/V_{1b} appearing in Eq. (25) is the only additional experimental data necessary for the correction, and can be obtained numerically directly from the controlling unit if the gain of the reference branch is regulated digitally, for example by means of a Digitally Controlled Attenuator (DCA) as indicated in Fig. 10. The snout correction calculated with Eq. (25) for the tested available module turned out to be 1.8%. The corrected value of the figure of merit is than $zT = 0.565$ (0.016).

A heuristic survey of calculated snout profiles for a number of reasonable device geometries has indicated that V_{1b} is typically greater than V_Ω, at least when $L_2 > L_1$, and that the Type B uncertainty with which they can be identified is conservatively smaller than 10% of the snout length. This

is comparable with the uncertainty of an *a priori* evaluation based on Eq. (16), given the unavoidable Type B contributions from data on geometry and material properties and from uncertainty in the model of constriction and spreading effects.

However, since the experimental approach seems to leave a positively biased uncertainty interval (from 0 to 10% of the snout) in the evaluation of V_Ω, it can be argued that this actually amounts to a Type B uncertainty of 5% of the snout on top of a positive bias of the same magnitude. In this perspective, the experimental approach would seem to be somewhat better than the mentioned *a priori* evaluation.

Furthermore, it can be noticed that such leftover bias is effectively an underevaluation of the snout length, which leads to an underevaluation of zT, and may therefore be partly compensated by the circularity bias, which leads instead to an overevaluation of zT, as quickly discussed at the beginning of this section. In the big-snout case of Figs. 6, 11, and 12, for example, the circularity bias on zT turns out to be about $+0.3\%$ if $zT^* = 1$, while the leftover snout bias on zT can be evaluated to be about -0.9%, with a Type B uncertainty of equal magnitude. In order to get this result, Eq. (21) must be rewritten multiplying S by 0.05, the mentioned 5% of S residual bias.

As a conclusion, it would be safe to state that the experimental approach to the snout correction would lead in this case to a zT value accurate to better than 1%.

It must be added here that both Type B uncertainty and mentioned biases scale with the snout length. The expected accuracy would then be comparatively improved for devices with a smaller snout.

All Type A uncertainty contributions, which arise in connection with S/N ratio, phase measurement resolution in the DPM and attenuation resolution in the DCA, are here assumed to be adequately small for the Type B uncertainty to dominate.

ACKNOWLEDGMENTS

The authors wish to thank Silvio Gualini for executing some of the experimental work which was taken into account in steering the direction of this mostly theoretical paper.

NOMENCLATURE

A = cross section of thermoelectric element (m^2)
C = frontal thermal capacity of a generic layer ($J\,m^{-2}\,K^{-1}$)
C_T = frontal thermal capacity of external layers ($J\,m^{-2}\,K^{-1}$)
f = frequency (Hz)
G = differential gain of the differential amplifier
i = electric current density ($A\,m^{-2}$)
j = imaginary unit
K = specific thermal conductance ($W\,m^{-2}\,K^{-1}$)
$\mathscr{K}$ = thermal conductance of the thermoelectric elements ($W\,K^{-1}$)
L = layer thickness (m)
r' = ratio between first and third term in Eq. (16)
r'' = ratio between second and third term in Eq. (16)
$\mathscr{R}$ = series electric resistance (Ω)
S = relative snout length referred to the dc Seebeck voltage
S^* = relative snout length referred to the porcupine body circle diameter
T = temperature (K)
V_ε = Seebeck voltage (V)
V_P = voltage drop on the thermoelectric module (V)
V_Ω = ohmic voltage drop (V)
y_0 = thermal admittance of the thermoelectric layer ($W\,m^{-2}\,K^{-1}$)
y_e = overall thermal admittance of the external layers ($W\,m^{-2}\,K^{-1}$)
y_T = total thermal admittance ($W\,m^{-2}\,K^{-1}$)
zT = true dimensionless figure of merit
zT* = dimensionless figure of merit in the lumped parameter approximation

Greek symbols

α = thermal diffusivity ($m^2\,s^{-1}$)
γ = phase difference between V_Ω and V_P
δ = relative circularity error of the porcupine body
ε = Seebeck coefficient ($V\,K^{-1}$)
ϕ = heat flux per unit surface ($W\,m^{-2}$)
λ = thermal conductivity ($W\,m^{-1}\,K^{-1}$)
ϑ = temperature excess
ρ_e = electric resistivity of thermoelectric material (Ω m)
Π = Peltier coefficient (V)
ψ = angle define by Eq. (17)
ω = angular frequency ($rad\,s^{-1}$)
ω_ι = characteristic angular frequency of layer i ($rad\,s^{-1}$)

Subscripts

0 thermoelectric material
1 electrical connection layer
2 isolator layer
ε referring to Seebeck voltage
ℓ referring to lumped parameter model
p referring to thermal pole

[1] T. C. Harman, J. Appl. Phys. **29**, 1373 (1958).
[2] T. C. Harman, J. H. Cahn, and M. J. Logan, J. Appl. Phys. **30**, 1351 (1959).
[3] A. De Marchi and V. Giaretto, Rev. Sci. Instrum. **82**, 034901 (2011).
[4] H. Iwasaki, M. Koyano, and H Hori, Jpn. J. Appl. Phys. **41**, 6606 (2002).
[5] H. Iwasaki, S. Yokoyama, T. Tsukui, M. Koyano, H. Hori, and S. Sano, Jpn. J. Appl. Phys. **42**, 3707 (2003).
[6] H. Iwasaki and H. Hori, in *Proceedings of the 24th International Conference on Thermoelectrics*, Clemson, SC (IEEE & ICT publisher, 2005, obtainable from p.wesling@ieee.org), p. 501.
[7] W. Kobayashi, W. Tamura, and I. Terasaki, J. Electron. Mater. **38**, 964 (2009).
[8] A. E. Bowley, L. E. J. Cowles, G. J. Williams, and H. J. Goldsmid, J. Sci. Instrum. **38**, 433 (1961).
[9] A. W. Penn, J. Sci. Instrum. **41**, 626 (1964).
[10] M. R. Campbell, C. A. Hogarth, and C. A. Hagger, Int. J. Electron. Commun. **19**, 571 (1965).
[11] C. L. Hapenciuc, F. J. Kahn, T. Borca-Tasciuc, and G. C. Wang, in *Proceedings of Material Research Society Symposium*, Boston, MA, 2003 (Cambrige University Press, New York, 2003), Vol. 793, p. 181.
[12] Z. Bian, Y. Zhang, H. Schmidt, and A. Shakouri, in *Proceedings of the 24th International Conference on Thermoelectrics*, Clemson, SC; (IEEE & ICT publisher, 2005, obtainable from p.wesling@ieee.org), p. 76.
[13] S. Fujimoto, H. Kaibe, S. Sano, and T. Kajitani, Jpn. J. Appl. Phys. **45**, 8805 (2006).

[14]A. Jacquot, M. Jägle, J. König, D. G. Ebling, and H. Böttner, in *5th European Conference on Thermoelectrics*, Odessa, Ukraine (European Thermoelectric Society, 2007, available online at:ect2007.its.org).
[15]E. E. Castillo, C. L. Hapenciuc, and T. Borca-Tasciuc, Rev. Sci. Instrum. **81**, 044902 (2010).
[16]G. Min and M. D. Rowe, Meas. Sci. Technol. **12**, 1261 (2001).
[17]G. Min, J. Electron. Mater. **39**(9), 1782 (2010).
[18]G. Gromov, D. Kondratiev, A. Rogov, and L. Yershova, in *Proceedings of the 6th European Workshop on Thermoelectricity of the European Thermoelectric Society*, Freiburg im Breisgau (European Thermoelectric Society, 2001, available online at: www.rmtltd.ru), p. 1.
[19]A. B. Putilin and E. A. Yuragov, Meas. Tech. **46**(12), 1173 (2003), [Izmeritel'naya Tekhnika **12**, 35 (2003)].
[20]A Degiovanni, B. Remy, and S. André, J. Therm. Sci. **11**(4), 359 (2002).
[21]Paul R. Clayton, *Fundamentals of Electric Circuit Analysis* (Wiley, New York, 2000), pp. 261–280.
[22]M. Abramowitz and I. A. Stegun, *Handbook of Mathematical Functions* (Courier Dover Publications, New York, 1972), pp. 1021–1029.